Title:

Evaluation of Plume Characteristics of Arc-heaters with Various Oxygen Injection Systems

Authors:

Makoto Matsui [a]*, Tomoyuki Ikemoto [a], Hiroki Takayanagi [b], Kimiya Komurasaki [a] and Yoshihiro Arakawa [b]

Affiliations:

[a] Department of Advanced Energy, The University of Tokyo

5-1-5 Kashiwanoha, Kashiwa, Chiba 277-8583, Japan

[b] Department of Aeronautics and Astronautics, The University of Tokyo

7-3-1 Hongo, Bunkyo, Tokyo 113-8656, Japan

*****Corresponding Author:*

Makoto Matsui

Department of Advanced Energy,

The University of Tokyo

5-1-5 Kashiwanoha,

Kashiwa, Chiba 277-8583, Japan

Fax: 04-7136-8583

Email: matsui@al.t.u-tokyo.ac.jp

Abstract:

Arc-heater plumes generated by various oxygen injection systems were investigated by laser absorption spectroscopy. Firstly, oxygen was directly injected into a high temperature cathode-jet region through a thoriated-tungsten hollow cathode. Although number density of atomic oxygen was increased, erosion of the cathode was too severe to maintain stable discharge. Then, zirconium was used as a cathode material to reduce cathode erosion by oxidation. As a result, stable discharge was maintained for three hours with pre-mixed argon-oxygen injection and number density of atomic oxygen was successfully increased.

Keywords:

Arc-heater, Atomic Oxygen, Zirconium Cathode, Laser Absorption Spectroscopy

1. Introduction

Atomic oxygen sources have been used in various research fields such as material processing [1], plasma etching and ashing for semiconductor [2], oxidation of nuclear waste [3], developments of thermal protection system for reentry vehicles [4] and protection of satellites structure in low earth orbit against degradation [5]. Various plasma devices have been developed to produce atomic oxygen as tabulated in **Table 1**. An arc-heater is one of the promising generators because of its high flux density as well as its high particle speed, high temperature and large flow area with uniformity. It can reduce experimental time dramatically; for example, deposition rate is enhanced more than one order higher than conventional CVD/PVD plasma sources [6] or fluence of incident atomic oxygen to satellites with one-year stay in low earth orbit can be simulated in less than a few decade minutes [7].

In our previous research, however, it was found that degree of dissociation in oxygen was much lower than that expected [8]. **Figure 1** shows a cross-section of conventional oxygen injection system. Oxygen is injected at the constrictor part separately from an inert working gas to prevent the cathode from oxidation.

Owing to this flow configuration, oxygen was neither enough mixed with the working gas nor dissociated in the constrictor region as schematically shown in **Fig. 1**. Although the oxygen was mixing in the plume, the dissociation rate was quite small because of the decrease in temperature, resulting in the low degree of dissociation in oxygen. In order to promote mixing, bi-throat anode design has been proposed [9].

In this study, arc-heaters with two kinds of oxygen injection systems were developed

and their performances were evaluated by laser absorption spectroscopy.

2. Experimental Method and Apparatus

2.1 Laser absorption spectroscopy

Laser absorption spectroscopy is applicable to optically thick plasma and does not require absolute calibration using a calibrated light source or a density reference cell. In addition, measurement system using a diode laser can be portable [12,13].

The relationship between laser intensity $I(\nu)$ and absorption coefficient $k(\nu, x)$ is expressed by the Beer-Lambert law as

$$\frac{\mathrm{d}I(\nu)}{\mathrm{d}x} = -k(\nu,x)I(\nu). \tag{1}$$

Here, ν is the laser frequency and x is the coordinate in the laser pass direction. Because distributions of absorption properties in plumes would be axisymmetric, local absorption coefficient $k(\nu, r)$ is obtained by the Abel inversion.

In our experimental conditions, Doppler broadening is several gigahertzes, which is two orders of magnitude greater than all other broadenings, including natural, pressure and Stark broadenings [13]. The absorption profile $k(\nu, r)$ is approximated as a Gaussian profile, expressed as

$$k(\nu,r) = \frac{2K(r)}{\Delta\nu_{\mathrm{D}}}\sqrt{\frac{\ln 2}{\pi}}\exp\left[-\ln 2\left\{\frac{2(\nu-\nu_0)}{\Delta\nu_{\mathrm{D}}}\right\}^2\right]. \tag{2}$$

Here, ν_0 is the center absorption frequency and $K(r)$ is the integrated absorption coefficient. $\Delta\nu_{\mathrm{D}}$ is the full width at half maximum of the profile and is related to the translational

temperature T, expressed as

$$\Delta\nu_{\mathrm{D}} = 2\nu_0\sqrt{\frac{2k_{\mathrm{B}}T}{mc^2}\ln 2}\,, \tag{3}$$

where m, c and k_{B} represent the mass of absorbers, velocity of light, and the Boltzmann constant, respectively.

Assuming Boltzmann relation between absorbing and excited states, integrated absorption coefficient is expressed as a function of the number density at the absorbing state $n_i(r)$ as,

$$K(r) = \int_{-\infty}^{\infty} k_\nu(r)\mathrm{d}\nu = \frac{\lambda^2}{8\pi}\frac{g_j}{g_i}A_{ji}n_i(r)\left[1-\exp\left(-\frac{\Delta E_{ij}}{k_{\mathrm{B}}T_{\mathrm{ex}}}\right)\right]. \tag{4}$$

Here, subscripts 'i' and 'j' denote the absorbing and excited states, respectively. λ, g, A, ΔE and T_{ex} are the absorption wavelength, statistical weight, Einstein coefficient, energy gap between the states and electronic excitation temperature, respectively. Transition data of target absorption lines (OI 777.19nm, ArI 842.46nm) are referred in Reference [14]. $\Delta E_{ij}/kT_{\mathrm{ex}}$ was so large in the plumes that stimulated emission can be neglected and Eq.(4) is approximated as,

$$K(r) = \frac{\lambda^2}{8\pi}\frac{g_j}{g_i}A_{ji}n_i(r)\,. \tag{5}$$

2.2 Measurement system

The block diagram of measurement system is shown in **Fig. 2**. A tunable diode-laser with an external cavity was used as a probe and an etalon, whose free spectral range is 1 GHz, was used as a wavemeter. Probe beam was lead to a window of vacuum chamber

through a multimode optical fiber. The fiber output was mounted on a one-dimensional traverse stage to scan the plume in the radial direction. At the other side of the chamber, the probe beam was focused on a photo-detector using a parabola mirror. This setup is possible to detect the probe beam without synchronizing the detector position with the laser scanning.

2.3 Arc-heaters and test conditions

2.3.1 Hollow injection

In this study, two kinds of oxygen injection system were developed. Firstly, instead of a conventional rod-shaped cathode, a hollow cathode was tested using thoriated-tungsten as cathode material. Oxygen is supplied through the cathode tip so as that oxygen passes through a high temperature cathode-jet region as shown in **Fig. 3**. The operating condition of the arc-heater is listed in **Table 2**. Compared with the conventional oxygen injection, oxygen flow rate at which arc discharge was sustainable was decreased by one-fifth.

2.3.2 Pre-mixed injection

Next, zirconium was used as cathode material instead of thoriated-tungsten to supply oxygen pre-mixed with argon [15-18]. Although the melting point of zirconium (2100 K) is lower than that of thoriated-tungsten (3680 K), it reacts with oxygen and forms an oxide ceramic layer on the cathode surface [15-18]. This layer composed of zirconia (zirconium dioxide) has high melting point of 3000 K and low vapor pressure, resulting in much lower erosion rate than that of thoriated-tungsten in the reactive gas flows [19].

A configuration of zirconium cathode is compared with conventional one as shown in

Fig. 4. Because thermal conductivity of zirconium is one-tenth as much as that of tungsten [19], the length from the zirconium cathode tip to the water-cooled cupper socket is 3 mm to prevent the cathode from melting. In addition, the tip of the cathode is shaped flatly. Before using the zirconium cathode, it was exposed in the conventional arc-heater plume to oxidize its surface for thirty minutes.

The operating condition of the arc-heater is listed in **Table 2**. Because of the flat-edge cathode, the discharge voltage was a little higher than that of cone-shaped cathode. Then, the current was reduced to 40 A. The mass flow was also reduced to conform the enthalpy to the previous experiment. Although the oxide ceramic layer is non-conductive at room temperature, discharge was successfully sustained because conductivity of the layer increased with the temperature.

3. Experimental Results

Figures 5, 6 compare distributions of meta-stable oxygen number density and translational temperature at the nozzle exit of the arc-heater in three kinds of injection. In the conventional injection [8], the peak of number density was located off axis and its value is 6.7×10^{15} m^{-3}. This annular peak indicates inadequate mixing process shown in **Fig. 1**. On the other hand, the temperature distribution has a peak on the axis and its value is 2300 K.

In the hollow injection, the number density distribution has a peak on the axis. Its maximum value is 2.3×10^{16} m^{-3}, which is four times as high as that in the conventional injection. The translational temperature distribution has a sharp peak on the axis and its value is around 1100 K, which is much lower than that in the conventional injection.

Because of the fluctuation of the plume, measurement error is relatively larger than the other injection plumes.

In the pre-mixed injection, the number density distribution also has a peak on the axis and its value is one-order magnitude higher than that of the conventional injection. The temperature distribution is almost flat and its value is around 1260 K, which is much lower than that in the conventional injection.

4. Discussion

4.1 Cathode erosion

In both hollow and pre-mixed injection, the number density of meta-stable oxygen was successfully enhanced. However, in the hollow injection, operating time was limited less than ten minutes because severe cathode erosion caused unstable discharge and sparks as shown in **Fig. 7**. The erosion length of the cathode was as much as 10 mm during one hour off and on operation as shown in **Fig. 8**. This is because the melting point of the cathode goes down from 3680 K (tungsten) to 1470 K (tungsten oxide) due to the oxidation. The severe erosion will cause plume contaminations as well.

On the other hand, in the pre-mixed injection, stable operation could be possible more than three hours as shown in **Fig. 9**. In addition, the cathode erosion is significantly smaller than that of the tungsten hollow cathode. **Figure 10** shows a photograph of the zirconium cathode before and after three hours operation. The erosion of the cathode is 1 mm, which corresponds to 5.1×10^{-5} g/s.

4.2 Estimation of degree of dissociation in oxygen

The degree of dissociation in oxygen is difficult to be deduced from the measured number density because the meta-stable state is not related to the ground state by Boltzmann equilibrium in arc-heater plumes [8]. Then, it was estimated assuming thermo-chemical equilibrium at discharge part and frozen flow through the nozzle expansion. In the calculation, seven chemical species Ar, O_2, O, Ar^+, $O2^+$, O^+ and e^-, and four chemical reactions $Ar \leftrightarrow Ar^+ + e^-$, $O_2 \leftrightarrow 2O$, $O \leftrightarrow O^+ + e^-$, $2O \leftrightarrow O_2^+ + e^-$ were considered. Their equilibrium constants were obtained from Reference [20, 21]. **Table 3** shows a calculation condition. The total temperature was estimated from the measured static one and designed Mach number of 2 assuming isentropic expansion. In the hollow injection, only oxygen was considered and partial pressure of oxygen deduced from measured total pressure was used because of oxygen flow around the cathode tip region. On the other hand, in the pre-mixed case, measured total pressure was used and ratio of mass fraction was matched to the experimental mass flow rate. **Figure 11** shows a calculation result in the pre-mixed injection. In this case, oxygen is dissociated around 2000 K.

Estimated degree of dissociation in oxygen is listed in **Table 3**. In the conventional injection, deduced total temperature is much higher than those in the others and then degree of dissociation is expected to be much higher. However, this higher temperature is due to the inadequate mixing process. This means that most of input energy is consumed not for the dissociation of oxygen but for the enhancement of translational temperature. The degree of dissociation by CFD considering the mixing process is 0.01% [8]. On the other hand, in both hollow and pre-mixed injection, the degree of dissociation reaches over 10 %.

However, considering the operating time and cathode erosion, pre-mixed injection is thought to be one of the potential candidates of high performance atomic oxygen generator.

5. Conclusion

Hollow injection of oxygen brought large increase in number density of atomic oxygen in the plume. However, its operating time was limited in less than ten minutes due to the severe cathode erosion. In case of pre-mixed injection with zirconium cathode, number density of meta-stable atomic oxygen was also increased with more than three hours operation. The degree of dissociation estimated from the measured temperature and thermo-chemical equilibrium calculation is 10.6 %, which is three orders magnitude higher than that of conventional injection. Then, zirconium cathode arc-heater with pre-mixed injection would be one of the potential candidates of high performance atomic oxygen generator.

Acknowledgements

This work was financially supported by Research Fellowships of the Japan Society for the Promotion of Science for Young Scientists.

References

[1] Ando, Y., et.al.; *J. IAPS*, 2004; 9: p85-90.

[2] Kiyohara, S., et.al.; *Nanotechnology*, 1999; 10: p385-388.

[3] Suzuki, M., et.al.; *J. Nucl. Sci. Technol.*, 1997; 34: p.1159-1170.

[4] Armenise, I., et.al.; *J. Spacecraft Rocket*, 2004; 41: p. 310-313.

[5] Peplinski, D. R., et.al.; *NASA CP-2340*, 1984.

[6] Tahara, H., et.al.; *Jpn. J. Appl. Phys*., 2003; 42: p3648-3655.

[7] Nishida, M., et.al.; *Trans. Japan Soc. Aero. Space Sci*., 1998;31: p123-133.

[8] Matsui, M., et.al.; *Vacuum*, 2004; 73: p.341-346.

[9] Auweter-Kurtz, M.; *NATO Research and Technology Organization proceedings*, 2000; RTO-EN-8: p.2A1-2A-20.

[10] Tagaya, M., et.al.; *AIAA J*, 1994; 32: p.95-100.

[11] Aoki, K., et.al.; *Toshiba Rev*., 2004; 55: p.17-20.

[12] Matsui, M., et.al.; *AIAA J*, 2005; 43: p.2060-2064.

[13] Matsui, M., Doctor Thesis, The University of Tokyo, 2005, web page address: http://www.kml.k.u-tokyo.ac.jp/papers/dissertation/matsui_d.pdf

[14] NIST Atomic Spectra Database, web page address: http://physics.nist.gov/cgi-bin/AtData/main_asd

[15] Marotta, A.; *J. Phys. D-Appl. Phys*., 1994; 27: p.49-53.

[16] Nemchinsky, V. A., et.al.; *J. Phys. D-Appl. Phys*., 2003; 36: p.704-712.

[17] Pustogarov, A. V., et.al.; *High Temp*., 1983; 21: p.178-183.

[18] Pustogarov, A. V., et.al.; *High Temp*., 1983; 21: p.936-940.

[19] Web Elements TM Periodic table, web page address: http://www.webelements.com/webelements/index.html

[20] Guputa R. N, et.al.; *NASA RP* 1232, 1990.

[21] Matsuzaki, R., et.al.; *Trans. Japan Soc. Aero. Space Sci*., 1987; 30: p.243-258.

Figure Captions:

Fig. 1 Schematic of conventional oxygen injection and mixing process.

Fig. 2 Block diagram of the measurement system.

Fig. 3 Cathode configuration of the hollow injection.

Fig. 4 Cathode configuration of the pre-mixed injection.

Fig. 5 Number density distributions of meta-stable atomic oxygen (3s5S).

Fig. 6 Translational temperature distributions.

Fig. 7 Photograph of a hollow injection plume.

Fig. 8 Erosion of thoriated-tungsten hollow cathode before and after operation.

Fig. 9 Photograph of a pre-mixed injection plume.

Fig. 10 Erosion of zirconium cathode before and after operation.

Fig. 11 Mole fraction and enthalpy by thermo-chemical equilibrium calculation

Table captions:

Table 1 Atomic oxygen generators.

Table 2 Operating conditions.

Table 3 Measured and estimated characteristics.

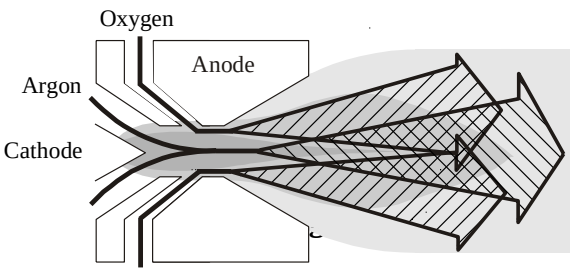
Oxygen
Anode
Argon
Cathode

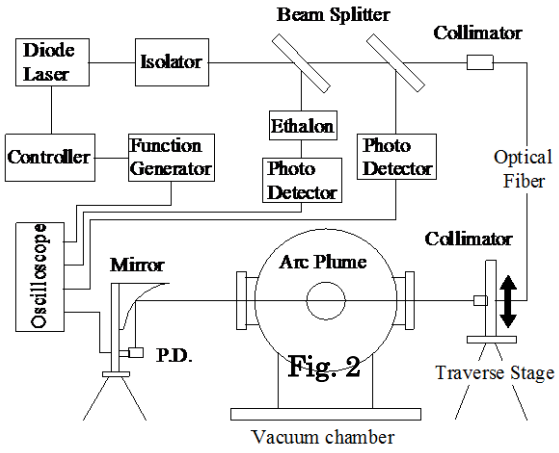
Beam Splitter
Collimator
Diode Laser
Isolator
Ethalon
Controller
Function Generator
Photo Detector
Photo Detector
Optical Fiber
Collimator
Oscilloscope
Mirror
Arc Plume
P.D.
Traverse Stage
Vacuum chamber

Fig. 2

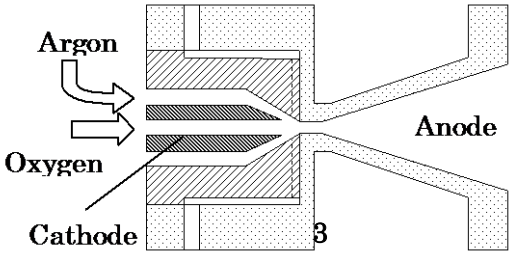
Argon
Oxygen
Cathode
Anode

3

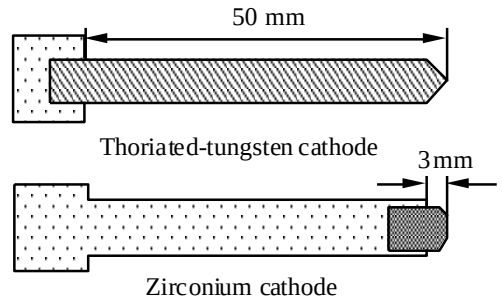
50 mm
Thoriated-tungsten cathode
3mm
Zirconium cathode

Fig. 4

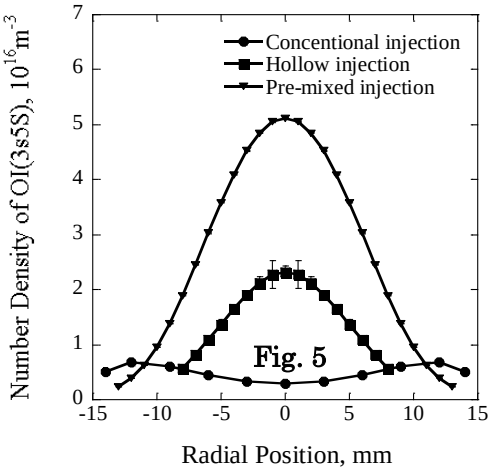
Concentional injection
Hollow injection
Pre-mixed injection
Number Density of OI(3s5S), 10^{16} m^{-3}
Radial Position, mm
0
1
2
3
4
5
6
7
-15
-10
-5
0
5
10
15

Fig. 5

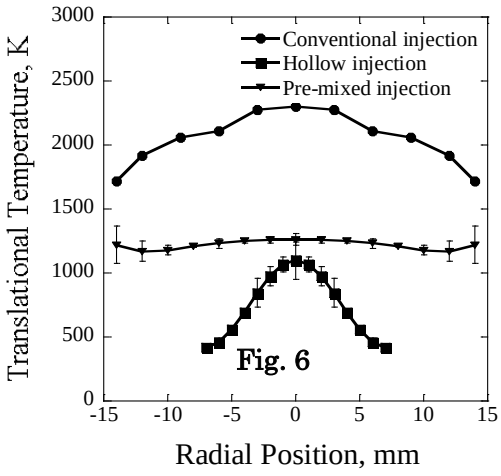
Translational Temperature, K
Radial Position, mm
Conventional injection
Hollow injection
Pre-mixed injection
3000
2500
2000
1500
1000
500
0
-15
-10
-5
0
5
10
15

Fig. 6

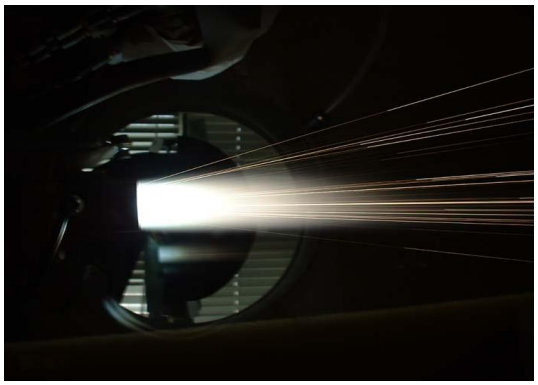

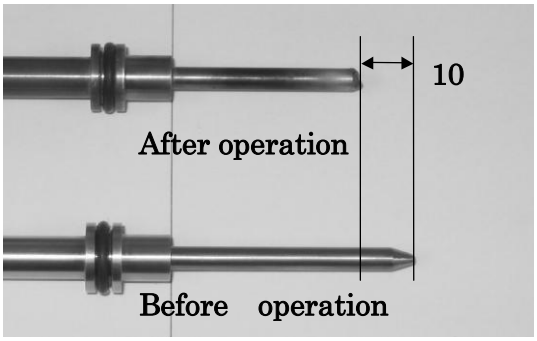
10
After operation
Before operation

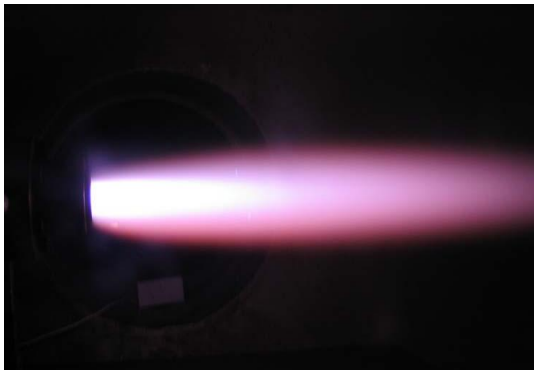

Fig. 9

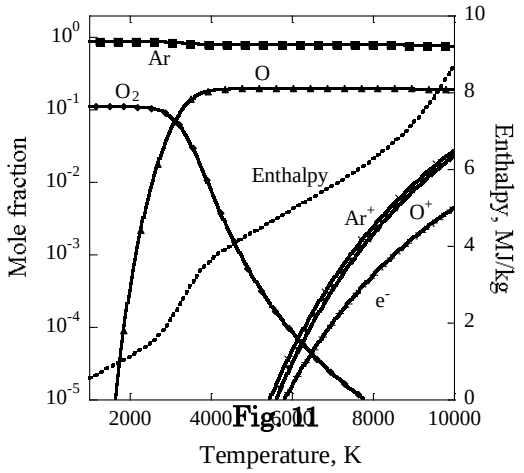
Ar
O
O2
Enthalpy
Ar+
O+
e-
Mole fraction
Enthalpy, MJ/kg
Temperature, K
10^0
10^-1
10^-2
10^-3
10^-4
10^-5
2000
4000
6000
8000
10000
0
2
4
6
8
10

Fig. 11

	Flux density	Energy	Mach number	Operational time
Arcjet [9]	~10^{19} $cm^{-2}s^{-1}$	~ 0.6 eV	~ 3	~ hour
Laser detonation [10]	~10^{14} $cm^{-2}s^{-1}$	~ 4.6 eV	> 5	~ μs (pulse)
Plasma processing [11] (ICP, ECR, SWP, HWP)	~10^{15} $cm^{-2}s^{-1}$	< 0.1 eV	Stationary	> day

Table 1

	Conventional	**Hollow**	**Pre-mixed**
Argon flow rate	6.0 slm	6.0 slm	4.0 slm
Oxygen flow rate	1.0 slm	0.2 slm	0.5 slm
Input power	1.0 kW (50A)	1.0 kW (50A)	1.0 kW (40A)
Thermal efficiency	60 %	39 %	39 %
Averaged Enthalpy	3.0 MJ/kg	2.2 MJ/kg	3.0 MJ/kg

Table 2

	Conventional	**Hollow**	**Pre-mixed**
Measured total pressure	80 kPa	80 kPa (O_2: 2.6 kPa)	70 kP
Measured static temperature	2300 K	1100 K	1260 K
Estimated total temperature	5300 K	1730 K	2720 K
Degree of dissociation	(CFD: 0.01 %)	11.3 %	10.6 %
Cathode erosion	< 0.1 mm/hour	10 mm/hour	~0.3 mm/hour

Table 3